Nanoscale

PAPER

View Article Online
View Journal | View Issue

Cite this: *Nanoscale*, 2025, **17**, 25664

Extended osteoarthritis pain relief with neosaxitoxin using alginate-core polymeric microparticles

Hengli Zhang,[a] Helna M. Baby,[a] Shingo Ishihara,[c] Chenzhen Zhang,[a] Jun Li,[c] Natalie S. Adamczyk,[c] Ezra M. Cohen,[d] Rachel E. Miller[c] and Ambika G. Bajpayee *[a,b]

Osteoarthritis (OA) is a leading cause of chronic pain, affecting millions worldwide. Conventional pharmacological treatments provide only short-term relief and pose risks with long-term use, highlighting the need for safer, sustained analgesic strategies. Voltage-gated sodium channels (Na_V), particularly $Na_V1.7$, are key mediators of OA pain and represent a promising therapeutic target. Neosaxitoxin (NSTX), a potent site-1 sodium channel blocker (S1SCB), exhibits high affinity for $Na_V1.7$. Clinical studies demonstrate that subcutaneous administration of NSTX can safely block sensory pain in healthy individuals, but its anesthetic effect is short-lived, limiting its clinical utility for OA. Here, we report the first use of NSTX for OA pain relief with a local intra-articular (IA) delivery approach. A low dose (10 pg) produced effective pain relief in a post-traumatic OA mouse model, as assessed by knee hyperalgesia testing. However, the effect persisted for only a few hours even with a 100-fold higher dose, highlighting the need for sustained delivery. To prolong this short-lived pain relief and overcome the challenges of encapsulating small, hydrophilic S1SCBs like NSTX, we developed a sustained-release platform using alginate–poly(lactic-*co*-glycolic acid) microparticles (AlgPLGA-MPs). Incorporation of a negatively charged alginate core in the inner aqueous phase enhanced NSTX encapsulation through electrostatic interactions and minimized burst release. IA injection of NSTX encapsulated AlgPLGA-MP in a murine OA model produced significant pain relief for up to one week. To further prolong joint residence time, the microparticle surface was functionalized with cationic avidin (AvAlgPLGA-MP) that reversed the net surface charge from anionic to cationic. This modification promoted electrostatic binding to negatively charged synovial matrix components and prolonged intra-joint retention time, while maintaining biocompatibility. Together, these results establish NSTX as a highly potent analgesic for chronic OA pain and present alginate-core PLGA microparticles as a safe and effective sustained-release platform. This delivery system holds broad translational potential for other small, hydrophilic analgesics and therapeutic agents.

Received 9th July 2025,
Accepted 7th October 2025

DOI: 10.1039/d5nr02912k

rsc.li/nanoscale

1. Introduction

Chronic pain affects approximately 20% of adults in the United States, with osteoarthritis (OA) being a major contributor.[1] Current pharmacological treatments—such as acetaminophen, NSAIDs, duloxetine, and opioids—offer only short-term relief and carry significant toxicity risks with prolonged use.[2] Consequently, there is a pressing need for safe, effective long-term therapies for OA pain.

Experimental models suggest that joint nociceptors are sensitized by pro-inflammatory mediators during joint damage, leading to peripheral sensitization.[3] This process activates transient receptor potential channels and voltage-gated sodium channels ($Na_V1.7$, $Na_V1.8$, and $Na_V1.9$), making them attractive drug targets for OA pain modulation.[4–6] The recent FDA approval of the $Na_V1.8$ inhibitor suzetrigine (JOURNAVX) underscores the therapeutic promise of sodium channel blockers.[7] Neosaxitoxin (NSTX), a site-1 sodium channel blocker (S1SCB) with high affinity for $Na_V1.7$, has also emerged as a promising candidate (Fig. 1A).[8–11] By acting at site-1, NSTX reversibly occludes sodium channel pores without inducing conformational changes, thereby avoiding neuronal desensiti-

[a]*Department of Bioengineering, Northeastern University, Boston, MA, USA. E-mail: a.bajpayee@neu.edu*
[b]*Department of Chemical Engineering, Northeastern University, Boston, MA, USA*
[c]*Department of Internal Medicine, Division of Rheumatology, Rush University Medical Center, Chicago, IL, USA*
[d]*Division of Immunology, Boston Children's Hospital, Harvard Medical School, Boston, MA, USA*

zation and plasticity that could lead to maladaptive adaptations over time.[12,13] Compared to its parent compound saxitoxin (STX), NSTX features an additional hydroxy group at the C11 position, enhancing its binding affinity to specific sodium channels.[14] Electrophysiological studies demonstrate that NSTX can inhibit action potentials in frog peripheral nerves by 50% at ~2 nM, making it five times more potent than STX and 1000–10 000 times more potent than local anesthetics like bupivacaine and lidocaine.[15–17] Notably, NSTX shows reduced affinity for the cardiac isoform $Na_V1.5$, minimizing risks of cardiac and neurotoxicity associated with traditional local anesthetics.[18–20]

NSTX has undergone clinical evaluation as a local analgesic. A high subcutaneous (S.C.) dose of 50 μg in healthy volunteers blocked heat pain for 3 hours and cold pain for 24 hours without adverse effects.[21] In a Phase I trial, 5–40 μg S.C. doses with buprenorphine and epinephrine modestly extended analgesia, but a single 10 μg dose lost its anti-nociceptive effect within an hour.[22] These findings support the safety and potential of NSTX but emphasize the need for sustained delivery strategies. To date, NSTX has not been evaluated for OA pain *via* intra-articular (IA) injection, and its efficacy at low doses remains unclear. Intra-joint depot formulations are needed to address rapid clearance and enable long-term relief.[23–25] Biodegradable materials like poly(lactic-*co*-glycolic acid) (PLGA) are widely used for controlled drug delivery and have FDA approval in products like Zilretta, a PLGA-based corticosteroid for OA pain.[26,27] However, encapsulating small, hydrophilic molecules in PLGA is challenging because these drugs tend to diffuse rapidly into the external aqueous phase during formulation.[28–30] This often leads to low encapsulation efficiency and a high initial burst release, which can compromise effective dosing. For instance, amoxicillin—a molecule similar to NSTX in both molecular weight and hydrophilicity—typically shows encapsulation efficiencies of only 4–35% using the double emulsion method, with an initial burst release exceeding 20%.[31] Therefore, it is critical to optimize PLGA-based delivery systems for high NSTX encapsulation and enable effective IA depot therapy for sustained OA pain management.

In this study, we evaluate the analgesic potential of NSTX for OA pain. We also develop a sustained-release intra-articular delivery system using alginate-PLGA microparticles (AlgPLGA-MP) and demonstrate that it can effectively provide prolonged pain relief in rodent models of post-traumatic OA. To further improve joint retention, we functionalized the particle surface with cationic avidin to enhance binding to negatively charged components of synovial fluid within the joint. Our findings, for the first time, demonstrate the feasibility of using NSTX-loaded microparticles for effective and sustained OA pain management, supporting their potential as a platform for delivering small hydrophilic analgesics.

Ambika G. Bajpayee

Ambika G. Bajpayee is an Associate Professor of Bioengineering at Northeastern University, where she directs the Molecular Bioelectrostatics and Drug Delivery Laboratory. Her research integrates bioelectrostatics, nanomaterials, and biomolecular engineering to develop targeted and sustained-release therapeutics for musculoskeletal repair. Her group designs charge-based peptide carriers, polymeric nanoparticles, and extracellular vesicle platforms to enhance drug transport across dense biological barriers. Dr Bajpayee earned her PhD in Mechanical Engineering from the Massachusetts Institute of Technology. Her honors include the US PECASE, NSF CAREER, NIH Trailblazer, and DoD Discovery Awards. Her translational work bridges fundamental science and clinical application through partnerships with academia, industry, and government agencies.

2. Methods

2.1 Materials

Resomer RG 505 (poly(D,L-lactide-*co*-glycolide) (PLGA) (M.W. 54–69 kDa, LA : GA = 50 : 50)), poly(ethylene glycol) methyl ether-*block*-poly(lactide-*co*-glycolide) (PEG-PLGA) (M.W. PEG 2 kDa, PLGA 10 kDa, LA : GA = 50 : 50), poly(vinyl alcohol) (PVA) (M.W. 30–70 kDa, 87–90% hydrolyzed), and TraceCERT neosaxitoxin solution were purchased from Sigma-Aldrich (St. Louis, MO). Alexa Fluor™ 488 Hydrazide, Lumiprobe™ Cyanine7 (Cy7) NHS ester, avidin, avidin-Texas Red™ conjugate, dimethyl sulfoxide (DMSO), dichloromethane (DCM), sodium alginate, Invitrogen™ DiBAC4(3) (bis-(1,3-dibutylbarbituric acid)trimethine oxonol) (bis-oxonol), and calcium chloride ($CaCl_2$) were obtained from Thermo Fisher Scientific (Waltham, MA). 1,2-Distearoyl-*sn-glycero*-3-phosphoethanolamine-*N*-[biotinyl(polyethylene glycol)-2000] (DSPE-PEG-biotin) was purchased from Avanti Polar Lipids (Alabaster, AL). The NSTX enzyme-linked immunoassay (ELISA) kit was obtained from Beacon Analytical Systems (Saco, ME). Neuro-2a mouse neuroblastoma cells were kindly provided by Dr Nitin Joshi (Brigham and Women's Hospital, Harvard Medical School). Veratridine was purchased from Tocris Bioscience (Bristol, UK). Propidium iodide (PI) was sourced from Thermo Fisher Acros Organics (Geel, Belgium). Low-glucose Dulbecco's modified Eagle's medium (DMEM) and phenol-red free DMEM were obtained from Cellgro (Manassas, VA). Fetal bovine serum (FBS) and penicillin–streptomycin–antimycotic (PSA) were purchased from Gibco (Grand Island, NY).

2.2 Formulation and characteristics of microparticles

2.2.1 AlgPLGA-MP and AvAlgPLGA-MP formulation. Two formulations, alginate-PLGA microparticles (AlgPLGA-MP) and

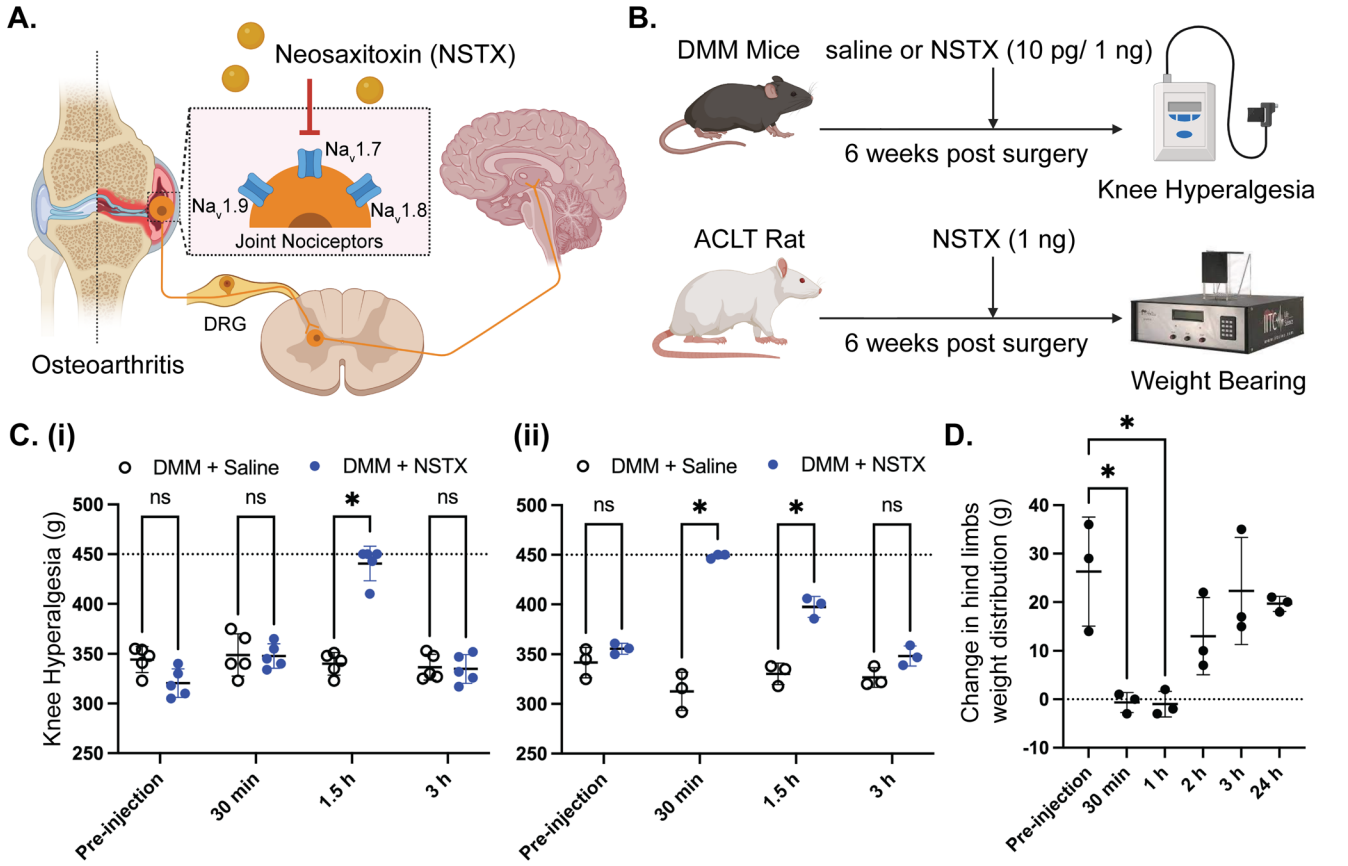

Fig. 1 NSTX in OA pain relief. (a) Schematic representation of the analgesic mechanism of NSTX in OA (scheme created with biorender.com). (b) Schematic depiction of NSTX intervention in two OA animal models—DMM mice and ACLT rats—along with their associated pain behavior analysis. (c) Knee hyperalgesia of 6-week post-DMM mice with NSTX or saline injection at doses of (i) 10 pg and (ii) 1 ng over a 3 hour time course. The withdrawal threshold baseline indicated by the dotted line (*$p < 0.05$ *vs.* saline; repeated measures two-way ANOVA with Bonferroni's multiple comparisons test). (d) Hindlimb weight-bearing differences were measured over a 24 hour time course following IA injection of 1 ng NSTX at 6 weeks post-ACLT surgery. The weight-bearing baseline indicated by the dotted line (*$p < 0.05$ *vs.* pre-injection; one-way ANOVA with Bonferroni's multiple comparisons test). Data are presented as mean ± SD.

avidin functionalized alginate-PLGA microparticles (AvAlgPLGA-MP), were prepared using the W/O/W double emulsion technique under sterile conditions, and the parameters for synthesis are listed in Table 1. To prepare NSTX encapsulated AlgPLGA-MP (NSTX-AlgPLGA-MP) and AvAlgPLGA-MP (NSTX-AvAlgPLGA-MP), the NSTX powder was mixed with 0–3% (w/v) sodium alginate in water and incubated overnight in a cold room to establish the inner aqueous phase. The oil phase was created by dissolving high molecular weight PLGA (54–69 kDa) in DCM (Table 1). The inner water phase and oil phase were mixed in a 1 : 10 (v/v) ratio and then subjected to ultrasonication for 3 minutes at 75 W to produce the primary emulsion (W_1/O). For AlgPLGA-MP synthesis, the outer aqueous phase was prepared by dissolving 3% (w/v) PVA in 25 mM Na_2HPO_4 solution, and adjusted to pH 10.75. This phase was homogenized with the primary emulsion using a handheld homogenizer at approximately 2500 rpm for 1 minute, forming the secondary emulsion ($W_1/O/W_2$). Subsequently, this emulsion was introduced into the continuous phase containing 2% (w/v) $CaCl_2$ and homogenized at the same speed for 2 minutes to form the $CaAlg_2$ inner core. After homogenization, the emulsion underwent a 12 hour evaporation process in a cold room. Microparticles were collected by centrifugation at room temperature for 15 minutes and washed 4 times with sterile water before freeze-drying. For AvAlgPLGA-MP, 0.15 mg of DSPE-PEG-biotin in 50 μL of DMSO was added before the second homogenization. This solution was then thoroughly mixed into a 2.5 mL $CaCl_2$-containing PVA solution for the preparation of the outer aqueous phase. Following evaporation and washing, the resulting formulation was incubated with avidin with various biotin to avidin mole ratios in 1 mL of 0.1 M bicarbonate buffer (pH 9.0) for 1 hour to facilitate surface modification of the PLGA microparticles with avidin.

2.2.2 Microparticle characterization. The zeta (ζ) potential of both formulations was quantified utilizing a Zetasizer. Additionally, the size distributions of the particles were assessed through confocal microscopy, while their morphological characteristics were examined *via* scanning electron microscopy (SEM). To verify the encapsulation of hydrophilic

Table 1 Parameters to formulate alginate-PLGA microparticles (AlgPLGA-MP) and avidin functionalized alginate-PLGA microparticles (AvAlgPLGA-MP)

Formulation/ parameters	AlgPLGA-MP	AvAlgPLGA-MP
Inner water phase (W_1) solvent	2% (w/v) alginate	2% (w/v) alginate
Oil phase (O) PLGA M. W.	54–69 kDa	54–69 kDa
Outer water phase (W_2)	3% PVA (pH 10.75)	3% PVA (pH 10.75) + DSPE-PEG-biotin
Biotin : avidin (mol)	N/A	1 : 0.5
$W_1/O/W_2$ volume ratio	1 : 10 : 500	1 : 10 : 500
NSTX : PLGA weight ratio	1 : 2500	1 : 1000

molecules within the PLGA layer, and the effective surface anchoring of avidin onto the PLGA layer, we adopted a strategy involving the incorporation of multiple fluorescent dyes for characterization *via* confocal microscopy. Specifically, Alexa Fluor 488, representing small hydrophilic molecules, was incorporated into the alginate solution, constituting the inner water phase (W_1). Furthermore, NHS-ester Cy7 was introduced into the oil phase. For the AvAlgPLGA-MP formulation, Texas Red-conjugated avidin was used for visualization. Confocal microscopy was used to confirm the distribution and localization of each layer within the formulated particles.

2.2.3 Encapsulation efficiency and loading capacity. To evaluate the encapsulation efficiency (EE%) and loading capacity (LC%) of NSTX within the formulations, the wash solution was collected during the process of formulation, and the washed particles were transferred to a pre-weighed tube prior to lyophilization to measure the yield weight of the lyophilized sample. After lyophilization, the particles in their powdered form were dissolved in dichloromethane (DCM). Subsequently, 500 μL of MilliQ nanopure water was added to this solution, followed by vortexing to facilitate the extraction of hydrophilic NSTX into the aqueous layer. The quantity of NSTX encapsulated within the particles was measured from the extracted aqueous layer, and the NSTX present in the wash solution was quantified separately using ELISA. The EE% and LC% were calculated as follows:

$$\text{Encapsulation efficiency}\,(\%) = \frac{\text{encapsulated NSTX}}{\text{encapsulated NSTX} + \text{washed away NSTX}} \times 100\%$$

$$\text{Loading capacity}\,(\%) = \frac{\text{encapsulated NSTX}}{\text{lyophilized sample weight}} \times 100\%$$

2.2.4 *In vitro* release profile of NSTX. The *in vitro* release profile of NSTX from both formulations was characterized using the sample-and-separate (SS) method.[32] Each analysis began by suspending 1 mg of microparticles in 1.5 mL of 1× PBS at pH 7.4. This suspension was then rotated at 60 rpm in a 37 °C incubator to simulate physiological conditions. At predetermined time points, the samples were centrifuged at 1000 rpm for 15 minutes to separate the supernatant from the pellet. The supernatant, containing released NSTX, was carefully collected for analysis and further experiments, while the pellet was resuspended in 1.5 mL of fresh PBS to continue the release process under the same conditions. The concentration of NSTX in the supernatant was quantified using an NSTX-specific ELISA kit (Beacon Analytical Systems, ME), adhering to the provided protocol. The cumulative release of NSTX was calculated using the following formula, where n represents the resuspension cycle at predefined time points:

$$\text{Cumulative release}\,(\%) = \frac{\sum_{n=0}^{N} \text{released NSTX}}{\text{encapsulated NSTX content}} \times 100\%$$

2.3 *In vitro* bioactivity

2.3.1 NSTX physiological stability. Stock solutions of NSTX were diluted to a concentration of 0.2 μg L^{-1} in 1× PBS and rotated at 37 °C at 60 rpm for two weeks. Every 1–3 days, 10% of the sample volume was collected and the concentration of NSTX was quantified using ELISA. The stability of free NSTX was normalized to the concentration measured on day 0, expressed in percentage. The stability of NSTX encapsulated within PLGA microparticles was assessed by adding both the cumulative release and the remaining content within the particles. Following the protocol outlined in method 2.2.4, NSTX-encapsulated PLGA particles were suspended and cultured. Samples were collected every day, and the supernatant was analyzed using ELISA to determine the released NSTX concentration. Additionally, 10% of the resuspended pellet was lysed after each centrifugation to measure the encapsulated NSTX content, while the remainder of the sample continued in the release experiment. The stability of the encapsulated NSTX was calculated using the following equation, where n represents the resuspension cycle:

$$\text{NSTX stability}_n\,(\%) = \frac{\sum_{n=0}^{N} \text{released NSTX} + 10\%\ \text{of NSTX remaining encapsulated}_n \times \frac{10}{0.9^n}}{\text{total encapsulated NSTX}} \times 100\%$$

2.3.2 Cytotoxicity analysis of NSTX and AlgPLGA-MP. Neuro-2a mouse neuroblastoma cells, gifted by Dr Nitin Joshi (Brigham and Women's Hospital, Harvard Medical School), were cultured in low-glucose DMEM supplemented with 1% penicillin/streptomycin/amphotericin (PSA) and 10% fetal bovine serum (FBS). After at least two passages, cells were seeded at a density of 5×10^3 cells per well in 96-well plates and cultured for 4 days. Cytotoxicity was assessed using the MTT assay after 24 hour treatments under various conditions. Cells were treated with culture media alone or media containing the supernatant from either blank AlgPLGA-MP or NSTX-AlgPLGA-MP released in the physiological environment. Additional treatment groups included media with 600 nM stock NSTX or DMSO at concentrations of 1% or 10%. After 24 hours, cells were stained with propidium iodide (PI; 10 μg mL^{-1} in PBS) for 5 minutes in the absence of light, followed by

a PBS wash. Fluorescence microscopy (Nikon) was used to visualize PI-stained non-viable cells, which appeared red.

2.3.3 Induced membrane potential recording – sodium sensitive *in vitro* experiment (IMPRESSIVE). To evaluate the bioactivity of released NSTX from NSTX-AlgPLGA-MP in blocking sodium channels, an assay of induced membrane potential recording – sodium sensitive *in vitro* experiment (IMPRESSIVE) was developed. This method involves monitoring the changes in cellular fluorescence using a membrane-potential-sensitive dye under confocal microscopy. After at least two passages, Neuro-2a cells were seeded at a density of 5×10^3 cells per well in a 96-well plate and cultured for 4 days. Prior to the IMPRESSIVE assay, the culture medium in each well was replaced with 100 μL of phenol-red free culture medium containing 30 nM bis-oxonol and incubated in a cell incubator for 30 minutes to allow for dye uptake. Cells exhibiting characteristic neuroblastoma morphology were selected for analysis. Fluorescence monitoring was conducted using a confocal microscope (LSM 880) equipped with a 10× objective lens, using an excitation wavelength of 493 nm and emission detection at 516 nm. After the stabilization of baseline fluorescence, 100 μL of 40 μM veratridine, a known sodium channel activator, was added to the wells leading to increased fluorescence due to sodium channel excitation. After 25–30 minutes, once the fluorescence signal had stabilized, the medium was replaced with one of the following: standard cell culture media, media containing 100 or 600 nM of stock NSTX, or media containing 600 nM of released NSTX from NSTX-AlgPLGA-MP as collected from the *in vitro* release experiment. Fluorescence measurements were continuously recorded for 19–20 minutes following the addition of these treatments. The recorded fluorescence data were then normalized to the average fluorescence value obtained during the 20–30 second interval post-treatment introduction.

2.4 Surgical procedure

2.4.1 Animals. All animal procedures were conducted in accordance with the USDA Animal Welfare Act, the Public Health Service Policy on Humane Care and Use of Laboratory Animals, and the Guide for the Care and Use of Laboratory Animals, as approved by the Institutional Animal Care and Use Committees (IACUCs) of Northeastern University and Rush University Medical Center. All *in vivo* experiments were performed on male C57BL/6 mice or male Lewis rats. The mice were bred in-house, provided with food and water, and randomly assigned to an OA model and experimental groups. Rats, aged 10 weeks and weighing 250–300 g, were obtained from Charles River Labs (Wilmington, MA, USA) and housed with food and water.

2.4.2 Destabilization of the medial meniscus (DMM), partial meniscectomy (PMX) and anterior cruciate ligament transection (ACLT) surgery. DMM or PMX surgeries were performed on the right knees of 10–12-week-old male C57BL/6 mice under isoflurane anesthesia, following previously described procedures.[33] In DMM surgery, the joint capsule was opened *via* medial parapatellar arthrotomy, the infra-patellar fat pad was dissected to expose the anterior medial compartment of the knee, and the anterior medial meniscotibial ligament was transected. Another cohort of mice underwent PMX surgery with an additional cut of approximately 1/3 to 1/2 of the anterior portion of the medial meniscus compared to DMM surgery.

ACLT or sham surgeries each were performed on the right knees of three 10-week-old male Lewis rats under isoflurane anesthesia, with a subcutaneous injection of buprenorphine (0.01 mg kg^{-1}). Similar to previously described procedures, a midline incision was made over the right anterior knee to expose the patellar tendon, followed by a medial parapatellar approach to enter the knee joint.[34] The patella was laterally displaced to expose and carefully transect the ACL. An anterior drawer test was performed to confirm the ACL transection. The joint capsule and skin incisions were then closed using 5-0 Vicryl sutures. For post-surgery treatment, meloxicam (2 mg kg^{-1}) was administered *via* subcutaneous injection immediately after surgery.

2.5 Pain behavior assessment

2.5.1 Knee hyperalgesia. Knee hyperalgesia in mice was quantitatively evaluated using a Pressure Application Measurement (PAM) device (Ugo Basile, Gemonio, Italy). Mice were securely held with the hind paw's knee flexed at a 90-degree angle, lightly stabilized with a finger. The PAM transducer was positioned manually on the medial knee, counterbalanced by the thumb on the lateral side, and force was applied gradually at a constant rate of 30 g s^{-1}, as guided by the PAM software. The withdrawal threshold was determined as the point where the mouse withdrew its knee, with a maximum force limit of 450 g per assessment. The average withdrawal force was recorded from two measurements per knee. Knee hyperalgesia was assessed in mice at 6 weeks post-DMM or PMX surgery, prior to intervention, to obtain baseline values. DMM mice were administered with a single intra-articular injection of free NSTX or saline. N = 3–5 DMM mice were used per condition. PMX mice were intra-articularly injected with NSTX-AlgPLGA-MP, NSTX-AvAlgPLGA-MP, blank AlgPLGA-MP, or blank AvAlgPLGA-MP on day 0 and day 2 after PAM measurement. N = 3–6 PMX mice were used per formulation condition. PAM measurements were continued for evaluating the knee hyperalgesia post-IA injection at predefined time points. Evaluators were blinded to group allocations.

2.5.2 Hindlimb weight bearing. The hindlimb weight-bearing measurement was used to evaluate pain behavior in ACLT rats. The measurements were taken using an incapacitance meter. ACLT rats were IA injected with free NSTX at 6 weeks post-surgery. N = 3 animals were used for weight-bearing measurements at predetermined time points. Rats, before surgery, underwent training to properly position themselves for 5 seconds on the incapacitance meter (IITC), with each hindlimb placed on separate sensor plates independently recording the weight bearing on each limb. A series of 15–-20 measurements were obtained at predetermined time points

following surgery or free NSTX intervention. The measurement was blinded to the observer to eliminate bias and ensure the objectivity of the data collected. Readings were carefully screened, and any measurement from an individual limb that represented less than 10% of the total body weight, or readings cumulated from both limbs for less than 30% of the total body weight, were excluded from analysis. The average of the valid measurements was calculated and used for the determination of weight distribution between the hindlimbs. The following formulations were applied for the calculation of weight distribution:

$$\text{Change in hindlimb weight distribution (g)} = \text{contralateral leg weight} - \text{treatment leg weight}$$

2.6 *In vivo* intra-articular joint retention

To assess the joint retention capability, 0.15 mg of NHS-ester-Cy7 was dissolved in the oil phase of each formulation (AlgPLGA-MP and AvAlgPLGA-MP) prior to the primary emulsification process. Male Lewis rats, aged 10 weeks, were anesthetized using isoflurane. The joint area on both legs was shaved and disinfected. Cy7 labeled formulations, AlgPLGA-MP and AvAlgPLGA-MP, were resuspended in 100 μL of sterile 1× PBS (pH 7.0) and IA injected into the legs. $N = 4$ rats were used per group. *In vivo* retention imaging was conducted using an *In Vivo* Imaging System (IVIS Spectrum). The radiant efficiency emitted from the joints was quantified over a period of 7 weeks. Radiant efficiency data were obtained from a fixed anatomical region of interest (ROI) at various time points for each experimental group.

2.7 Histopathological analysis

Bilateral knee joints of PMX mice were harvested at 2 weeks post-injection, decalcified in 14% EDTA, fixed in formalin, and paraffin embedded. Coronal or sagittal mid-joint sections (5 μm) were stained with H&E or Safranin O/Fast Green (Saf-O) using standard protocols described before.[35] Synovial pathology in four regions—medial tibial (MT), medial femoral (MF), lateral tibial (LT), and lateral femoral (LF) gutters—was assessed for three features: lining hyperplasia (lining layer thickness, cell layers), subintimal cellularity (cellular density), and subintimal fibrosis (extracellular matrix density).

2.8 Statistical analysis

In vivo knee hyperalgesia for $N = 3$–6 per group of PTOA mice, and intra-articular joint retention data for $N = 4$ per group of healthy rats were analyzed using repeated-measures two-way analysis of variance (ANOVA) with Bonferroni *post hoc* tests. Weight-bearing asymmetry for $N = 3$ ACLT rats was assessed *via* one-way ANOVA followed by Tukey's *post hoc* test. $N = 4$–-6 histology sections per condition were measured for synovitis histopathology scores using multiple unpaired *t*-tests corrected *via* the Benjamini–Krieger–Yekutieli method. The data are expressed as mean ± SD, with $p < 0.05$ considered statistically significant.

3. Results

3.1 NSTX exhibits short-term pain relief in DMM mouse and ACLT rat models

The analgesic effect of NSTX for chronic OA pain was evaluated using two PTOA preclinical animal models (Fig. 1B). Healthy mice exhibited a baseline maximum knee hyperalgesia threshold of 450 g, which declined to approximately 350 g at 6 weeks post-DMM surgery with the progression of chronic OA pain. A theoretical minimum dose of 10 pg was tested, corresponding to the half-maximal inhibition of action potential duration (APD_{50}) of NSTX in the physiological environment.[15] Notably, this low dose provided significant pain relief within 1.5 hours post-injection, but the effect was not sustained (Fig. 1C-i). To assess whether a higher dose could extend pain relief, the IA dose was increased by 100-fold to 1 ng, which restored the hyperalgesia threshold to the baseline within 30 minutes in DMM knees and remained significantly improved compared to the saline-injected control for up to 1.5 hours. This effect, however, lasted only 3 hours post-injection and was accompanied by mild lethargy in the animals (Fig. 1C-ii). This indicates that a 100 times higher dose did not significantly extend the duration of relief, likely due to rapid drug clearance from the joint.

A similar pain relief effect was observed in the ACLT rat model. ACLT rats exhibited persistent hindlimb weight distribution imbalances compared to both sham and naïve controls, which maintained values near zero (Fig. S1, SI). At 6 weeks post-surgery, IA injection of 1 ng NSTX into the ACLT knee significantly reduced weight distribution differences to near zero within 30 minutes to 1 hour, indicating effective pain relief (Fig. 1D). However, this effect was transient and completely lost after 2 hours.

3.2 Synthesis and optimization of PLGA-based formulation to encapsulate NSTX

To prolong the analgesic effect and overcome the challenges of encapsulating hydrophilic S1SCBs, PLGA-based microparticles were developed and optimized for sustained release. Although various formulation parameters of the double emulsion method were fine-tuned, the encapsulation efficiency (EE%) of NSTX remained low, accompanied by a substantial burst release of nearly 40% (Fig. S2, SI). To address this, alginate, a negatively charged polymer, was introduced into the formulation to enhance encapsulation of hydrophilic NSTX. The presence of alginate within the inner aqueous phase creates a viscous solution that prevents the escape of NSTX molecules during the emulsification process (Fig. 2A).[36,37] Additionally, the net positive charge of NSTX exhibits electrostatic interactions with alginate to improve retention during formulation (Fig. 2B). The subsequent addition of divalent calcium ions during the secondary emulsion allows for exchange with sodium ions to crosslink alginate and form a solidified inner alginate core after droplet formation (Fig. 2C). Formulations containing alginate (AlgPLGA-MP) exhibited significantly higher encapsulation

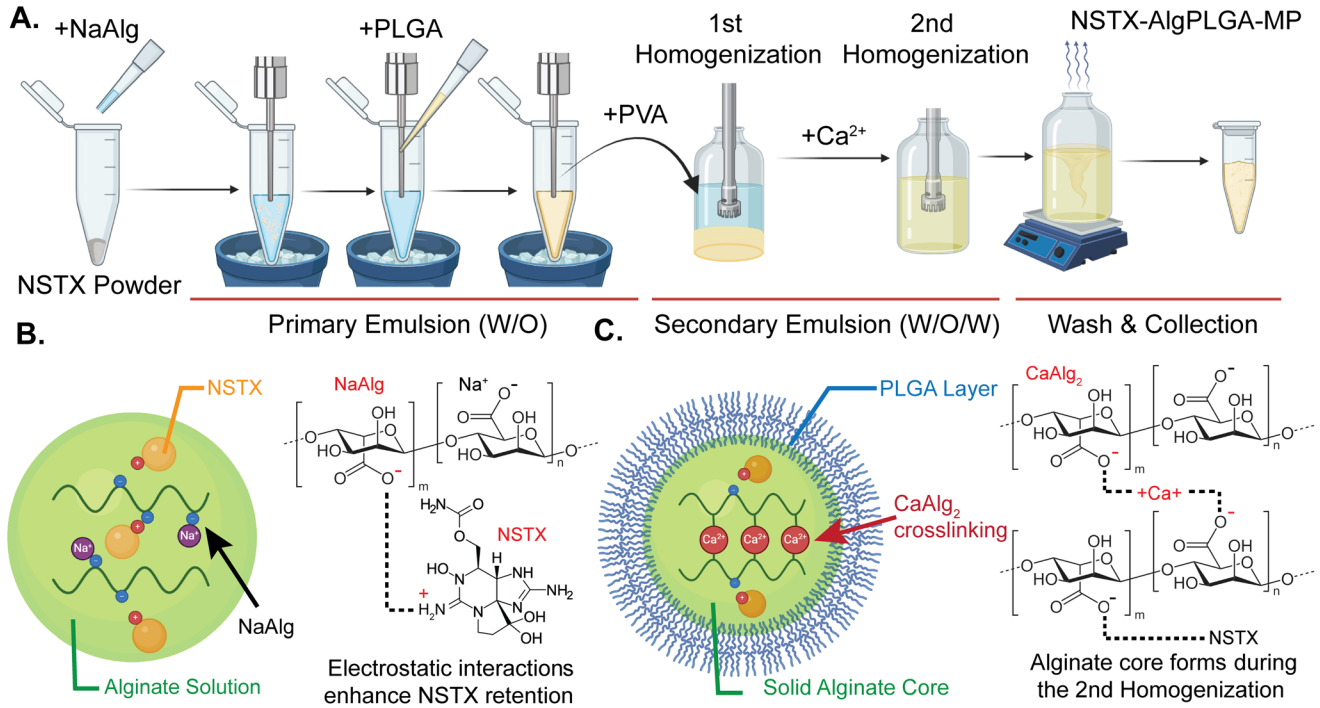

Fig. 2 Schematic illustrating the synthesis of NSTX encapsulated alginate-PLGA double core microparticles (AlgPLGA-MP) and the mechanism of core solidification. (a) NSTX-AlgPLGA-MP are synthesized using a W/O/W double emulsion method. (b) Schematic illustration of the NSTX-alginate droplet in the primary emulsion. Negatively charged alginate can electrostatically interact with the guanidinium group of NSTX, reducing its escape. (c) Schematic illustration of NSTX-AlgPLGA-MP. During the secondary emulsion process, calcium ions replace sodium ions in the inner core, cross-linking the alginate and forming a solidified alginate core within the PLGA shell (schemes created with biorender.com).

efficiencies than water-only formulations, resolving the issue of poor NSTX encapsulation. Notably, with 2% alginate, the EE% reached 89.6 ± 4.3%, the highest among all tested formulations (Fig. 3A and Table 2).

3.3 Characterization of AlgPLGA-MP

Confocal microscopy images demonstrated the uniform distribution of fluorescently labeled particles without aggregation, where dual-labeled particles are shown overlaid with the brightfield background and distinctly showed a structure with an alginate core (green fluorescence) surrounded by a PLGA layer with near-infrared (NIR) fluorescence indicated in blue (Fig. 3B). The average size of the particles was 9.9 ± 5.8 μm, with the majority falling within the 5–15 μm range (Fig. 3C and Table 2). As for the release profile, the 1% alginate formulation exhibited a high burst release of 21.9% ± 1.6% within 4 hours, whereas the 2% alginate formulation showed a much lower burst release of 4.8% ± 1.0%, indicating better initial retention of NSTX in the 2% formulation (Fig. 3D). The 1% alginate formulation followed a near-logarithmic release profile for the first 3 weeks, with an increased release rate between weeks 3 and 5. Conversely, the 2% alginate formulation released NSTX at a gradual rate of about 5% per day during the first 3 days, followed by a slower release of approximately 0.34% per day until week 4. Between weeks 4 and 5, 23% of NSTX was released. This delayed release likely results from the double-core structure of alginate and PLGA, where the degradation of the PLGA layer allows the alginate-NSTX core to be fully released. The morphology of the particles during *in vitro* release was analyzed using SEM (Fig. 3E). Freshly formulated particles exhibited a rough "stone-like" shape, likely due to the sticky nature of alginate, which prevented the formation of uniformly round particles during homogenization. After one week of release, some debris was observed due to particle hydrolysis, but most particles retained their original morphology (Fig. 3E-iii). NSTX release appeared to occur through expanded, hydrolyzed pores. In subsequent weeks, the particles began to disintegrate and expand their inner alginate core, facilitating additional NSTX release. Taken together, 2% alginate was selected for the optimized AlgPLGA-MP formulation in the subsequent *in vitro* and *in vivo* experiments.

3.4 NSTX and AlgPLGA-MP are non-cytotoxic and NSTX remains stable in NSTX-AlgPLGA-MP

The MTT assay confirmed that NSTX and AlgPLGA-MP are safe as the neuroblastoma cells treated with the AlgPLGA-MP released supernatant or free NSTX showed cellular viabilities higher than 90% similar to the untreated control conditions (Fig. 4A). In live/dead staining, a significant number of non-viable and detached cells were observed in the DMSO-treated group, whereas the vehicle, NSTX, and NSTX-AlgPLGA-MP treated groups showed minimal cell death (Fig. 4B). Both

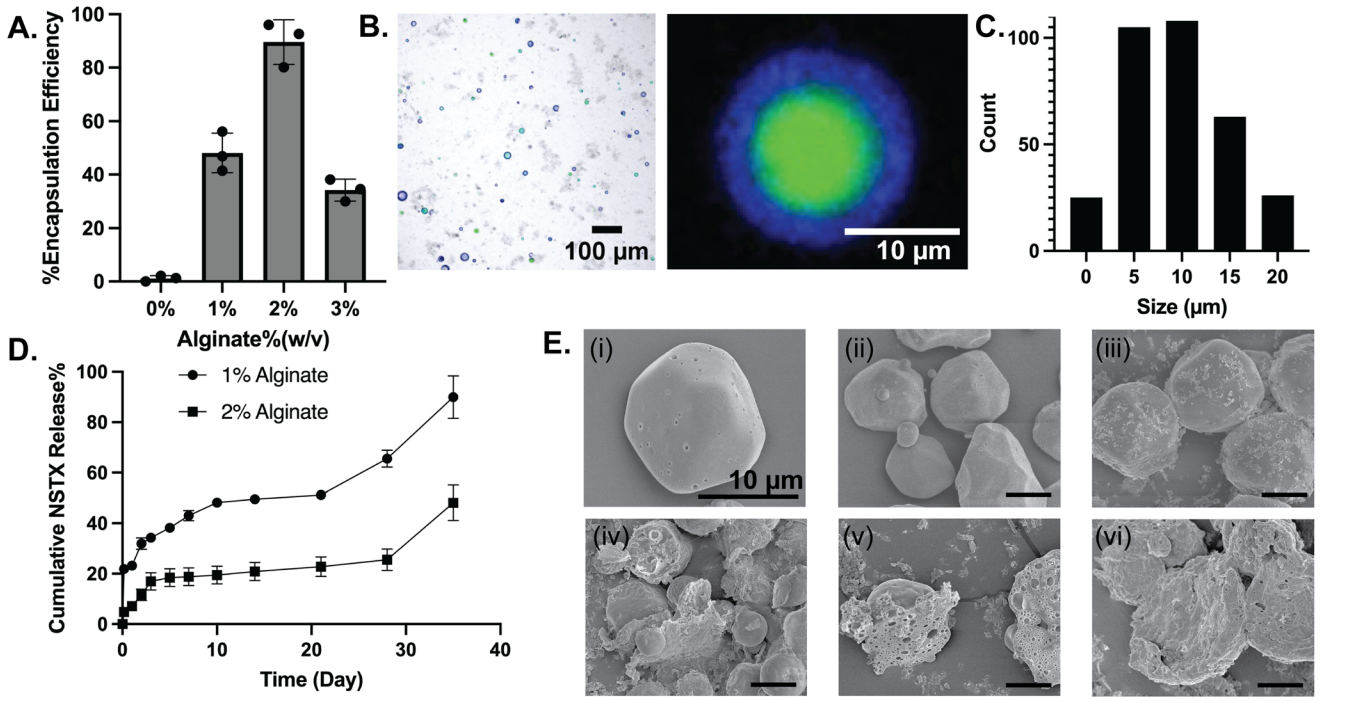

Fig. 3 Characterization of NSTX-AlgPLGA-MP. (a) Encapsulation efficiency (ee%) of NSTX in AlgPLGA-MP with varying alginate concentrations from 0–3% (w/v). (b) Confocal images of AlgPLGA-MP overlaid on the brightfield background with Alexa Fluor 488 (green) loaded in the alginate core and Cy7 (blue) in the PLGA layer. (c) Size distribution of AlgPLGA-MP. (d) *In vitro* cumulative release profiles of NSTX-AlgPLGA-MP formulated with 1% and 2% alginate in the physiological environment. (e) SEM images of AlgPLGA-MP illustrating the morphology of (i) the representative single particle, (ii) before release, and particles released for (iii) 1 week, (iv) 2 weeks, (v) 3 weeks, and (vi) 1 month in the physiological environment. Scale bar = 10 μm.

Table 2 Size, zeta potential, encapsulation efficiency (EE%), and loading capacity (LC‰) of NSTX encapsulated alginate-PLGA microparticles (NSTX-AlgPLGA-MP) and NSTX encapsulated avidin functionalized alginate-PLGA microparticles (AvAlgPLGA-MP)

Formulation	Size (μm)	Zeta potential (mV)	EE%	LC‰
NSTX-AlgPLGA-MP	9.9 ± 5.8	−26.4 ± 5.8	89.6 ± 4.3	2.4 ± 0.1
NSTX-AvAlgPLGA-MP	7.6 ± 4.0	20.1 ± 10.4	18.2 ± 1.1	1.9 ± 0.1

assays consistently demonstrated that neither AlgPLGA-MP nor NSTX poses cytotoxicity concerns.

NSTX has been found to be unstable during long-term storage at various low temperatures, in contrast to STX.[38] To determine whether NSTX encapsulated within AlgPLGA-MP remains stable, an *in vitro* release experiment was conducted. While free NSTX degraded over time in the physiological environment, the sum of the released and retained NSTX content within AlgPLGA-MP remained consistent with the original content (Fig. 4C).

3.5 AlgPLGA-MP released NSTX is bioactive

An induced membrane potential recording – sodium sensitive *in vitro* experiment (IMPRESSIVE) assay was developed to evaluate the bioactivity of released NSTX in sodium channel blockade (Fig. 4D-i). Neuro-2a neuroblastoma cells, rich in sodium channels, were selected and treated with bis-oxonol, a cell-penetrating membrane potential-sensitive dye. Upon introduction of the sodium channel activator veratridine, sodium ion influx occurs, leading to an increase in the membrane potential.[39–41] To restore homeostasis, bis-oxonol from the extracellular medium enters the cells, resulting in increased fluorescence that stabilizes within 10–20 minutes. After introduction of 600 nM NSTX at 30 minutes, a significant decrease in fluorescence was observed, indicating a reduction in membrane potential consistent with its sodium channel-blocking activity (Fig. 4D-i–iii).

The IMPRESSIVE assay demonstrated a dose-dependent response to NSTX (Fig. 4D-iv). Under control conditions, fluorescence remained at approximately 90% after 18 minutes (Fig. 4D-iv, black). The addition of 100 nM NSTX reduced fluorescence to approximately 50% after 18 minutes (Fig. 4D-iv, orange). At 600 nM, fluorescence decreased to about 20% of its initial value, indicating a potent sodium channel blockade (Fig. 4D-iv, blue). When comparing the response of NSTX released from NSTX-AlgPLGA-MP to that of stock NSTX, the fluorescence curves were nearly identical (Fig. 4D-iv, red). This finding confirms that encapsulated NSTX retains its bioactivity post-release, effectively blocking sodium channels *in vitro*.

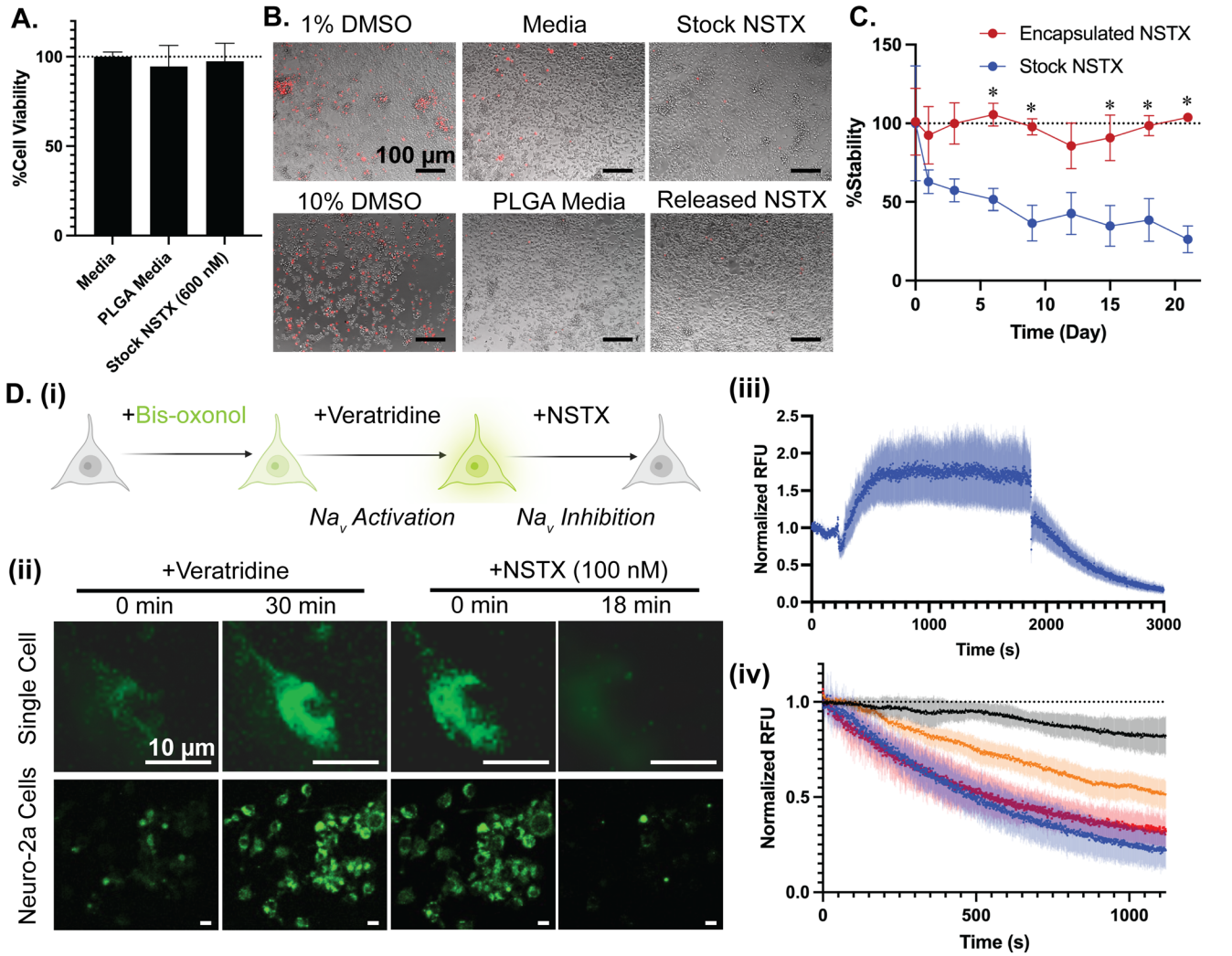

Fig. 4 Cytotoxicity, stability, and bioactivity of AlgPLGA-mp encapsulated NSTX. (a) Neuro-2a cell viability after 24 hour treatment with media, vehicle supernatant, or stock NSTX, assessed using the MTT assay. (b) Pi-stained images of Neuro-2a cells after 24 hour treatment with 1% DMSO, 10% DMSO, media, vehicle supernatant, stock NSTX, or NSTX-AlgPLGA-MP released NSTX. (c) Stability of free and encapsulated NSTX in the physiological environment over time measured with ELISA. (*$p < 0.05$ *vs.* stock NSTX; repeated measures two-way ANOVA with Bonferroni's multiple comparisons test). Data are presented as mean ± SD. (d) Impressive assay: (i) schematic of the steps and the corresponding cell fluorescence intensity change, (ii) representative fluorescence images of cells treated with veratridine and 100 nm of NSTX, (iii) fluorescence changes value after introducing veratridine and following replacement of 600 nm of stock NSTX, (iv) fluorescence changes after replacement with media (black), stock NSTX in 100 nm (orange) and 600 nm (red), or NSTX-AlgPLGA-MP released NSTX (blue). The Na$_v$ activated cell RFU baseline is indicated by the dotted line.

3.6 NSTX-AlgPLGA-MP exhibits pain relief in the PMX mouse model for almost a week

To further evaluate the efficacy of NSTX-AlgPLGA-MP for pain relief, formulations were administered as IA injections in PTOA PMX mice. Both 10 pg and 1 ng free NSTX resulted in short-term pain relief, which was discernible only at 1.5 h post-administration. Additionally, the high 1 ng dose led to undesirable lethargy and other side effects in animals. Therefore, to facilitate one-time depot delivery of NSTX-AlgPLGA-MP, a moderate dose of 100 ng was chosen based on the minimum effective dose and the slowest release rate of 0.19% per day in the first week of the *in vitro* release profile. However, due to limitations in small injectable volumes in mouse knee joints and aggregation issues arising from high concentrations of NSTX-AlgPLGA-MP in a 30G needle, a total of 84 ng of NSTX-encapsulated formulation was administered *via* two intra-articular injections—42 ng each on day 0 and day 2.

Prior to injection, OA-induced knee hyperalgesia resulted in a withdrawal threshold of 323.7 ± 18.2 g. After injection, within 30 minutes, the burst release of NSTX significantly alleviated pain compared to blank AlgPLGA-MP (Fig. 5A). The analgesic effect gradually increased the withdrawal threshold, peaking at 1.5 hours post-injection, but then gradually diminished. By 24 hours post-injection, the pain relief effect was no

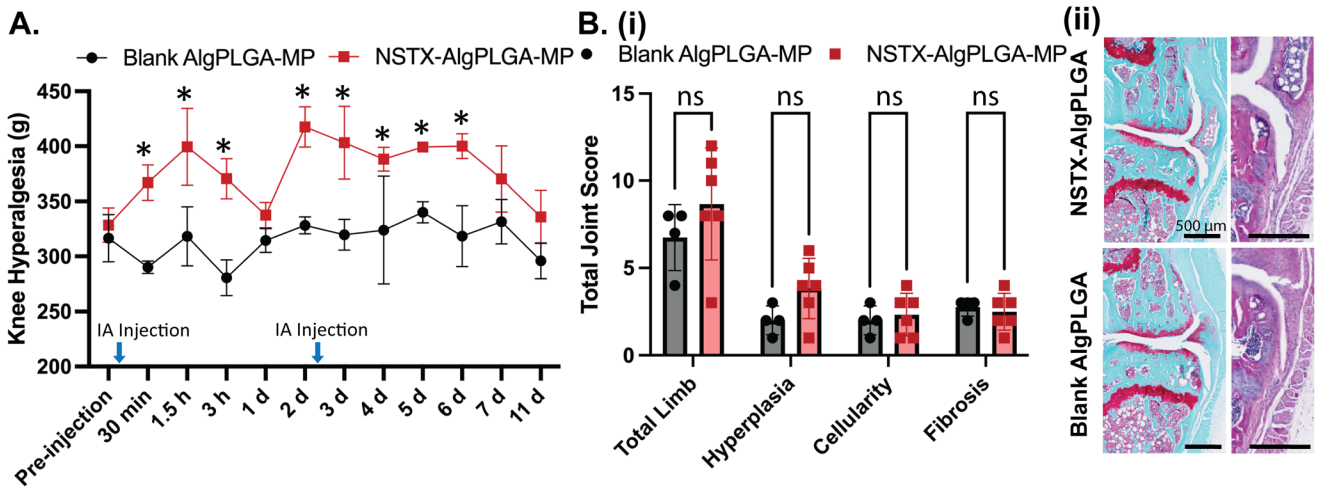

Fig. 5 *In vivo* pain relief and histopathology of NSTX-AlgPLGA-MP in PMX mice. (a) Analgesic effect in 6-week post-PMX mice treated with NSTX-AlgPLGA-MP *vs.* blank AlgPLGA-MP over 11 days. (*$p < 0.05$ *vs.* blank AlgPLGA-MP; repeated measures two-way ANOVA with Bonferroni's multiple comparisons test). (b) (i) Synovitis pathological scoring at 2 weeks post injection of NSTX-AlgPLGA-MP or blank AlgPLGA-MP and (ii) representative histology images (Saf-O/H&E) of medial joints and medial tibial synovitis respectively. Multiple unpaired *t*-tests corrected with Benjamini–Krieger–Yekutieli correction, mean ± SD.

longer detectable, as the initial relief was primarily driven by the burst release of NSTX from AlgPLGA-MP. Similar to the experiments with free NSTX, this transient effect faded due to rapid clearance of the released drug from the joint.

However, pain relief re-emerged at 48 hours post-injection, with a withdrawal threshold of 417.5 ± 18.5 g, significantly higher than vehicle control groups which landed at 328.3 ± 7.7 g (Fig. 5A). After 2 days, as the PLGA polymer started hydrolyzing for bulk release, sustained NSTX release maintained higher withdrawal thresholds in a level around 400 g through days 2–6, remaining significantly above vehicle controls. However, due to progressive particle clearance and the minimal dosing without accounting for *in vivo* particle loss, the slow-release phase beyond day 6 no longer provided sufficient NSTX to sustain statistically significant pain reduction, though thresholds remained slightly elevated compared to vehicle-treated mice. This suggests that NSTX delivered *via* AlgPLGA-MP elicits both immediate pain relief through an initial burst release and extended relief through sustained polymer hydrolysis.

Additionally, cartilage pathology in the medial mid-joint area showed no significant differences between the vehicle and NSTX-AlgPLGA-MP treated groups (Fig. 5B). This indicates that NSTX-AlgPLGA-MP does not exacerbate cartilage damage induced by OA. Given that synovial pathology is closely associated with OA pain and considering that NSTX-AlgPLGA-MP provided nearly a week of pain relief in PMX mice, synovitis pathology was evaluated in the synovial gutters of the mid-joint region. As shown in Fig. 5B-i, there were no significant differences in the combined histopathological scores across all four regions between the blank AlgPLGA-MP and NSTX-AlgPLGA-MP groups. These findings suggest that NSTX-AlgPLGA-MP does not increase joint damage or severity. However, to maintain effective analgesia over longer periods, a higher dose or delivery systems with longer joint-residence time may be necessary to compensate for particle clearance and the declining release rate.[23–25]

3.7 AvAlgPLGA-MP reversed the surface charge and exhibited longer joint retention

Avidin was anchored on the surface of AlgPLGA-MP to form cationic AvAlgPLGA-MP for the purpose of extending the intra-joint retention time.[42–46] While the zeta potential of AlgPLGA-MP is highly negative, it increased progressively in proportion to the introduced avidin (Fig. 6C). The introduction of avidin on the particle surface at a 50% molar ratio relative to biotin reversed the net negative charge of AlgPLGA-MP to about +20 mV. This is referred to as AvAlgPLGA-MP (Fig. 6A). The cationic NSTX-AvAlgPLGA-MP reversed the charge from −26.4 ± 5.8 to 20.1 ± 10.4 mV with a similar size and loading capacity (LC‰) compared with NSTX-AlgPLGA-MP (Table 2). Confocal imaging of AvAlgPLGA-MP indicates that Texas Red-labeled avidin formed a distinct layer covering AlgPLGA-MP, indicating the successful surface anchoring of avidin (Fig. 6B). To rule out nonspecific binding to alginate, particles without alginate were synthesized and imaged where the representative Z-stack image illustrated that avidin was localized on the outer layer (Fig. S3, SI).

Following IA injection in healthy rats with NIR fluorescent dye Cy7-labeled formulations, AvAlgPLGA-MP with about 5 μM avidin exhibited higher retention compared to AlgPLGA-MP, with significantly greater fluorescence observed at 2 weeks post-injection. After 3 weeks, fluorescence levels in both groups had dropped with no significant retention difference (Fig. 6D).

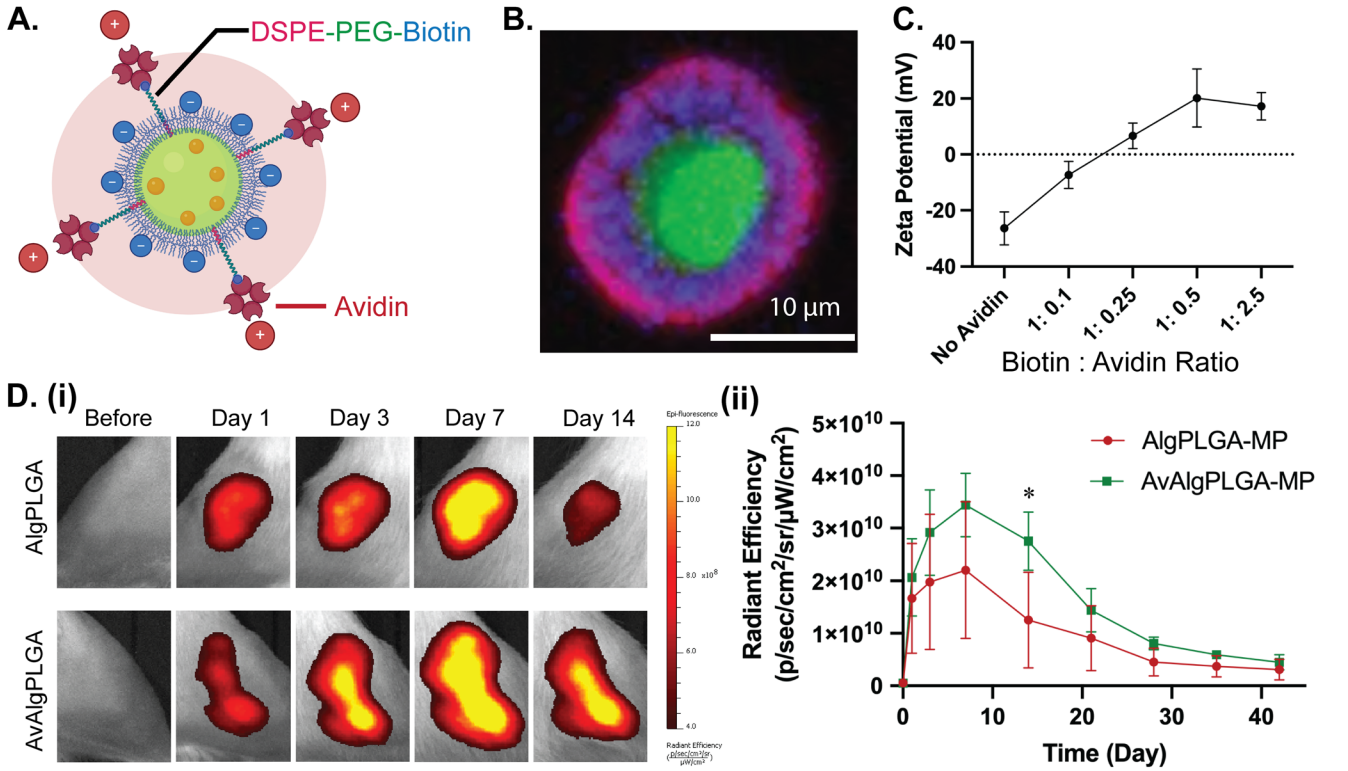

Fig. 6 Cationic avidin-coated AlgPLGA-MP (AVAlgPLGA-MP) enhances joint retention and therapeutic effect. (a) Schematic illustration of AvAlgPLGA-mp. (b) Confocal image of AVAlgPLGA-MP showing Alexa Fluor 488 (green) in the alginate core, Cy7 (blue) in the PLGA layer, and avidin-Texas Red (red) coating on the surface. (c) Surface zeta potential of microparticles at varying biotin-to-avidin ratios. (d) (i) Representative IVIS images of healthy rat legs injected with the same dose of Cy7 loaded AlgPLGA-MP or AVAlgPLGA-MP over 2 weeks and (ii) their radiant efficiency changes over 7 weeks (*$p < 0.05$ *vs.* AlgPLGA-MP; repeated measures two-way ANOVA with Bonferroni's multiple comparisons test). Data are presented as mean ± SD.

4. Discussion

In this study, we report the first use of NSTX for OA pain relief through local intra-articular (IA) delivery, together with the development of an alginate-PLGA microparticle (AlgPLGA-MP) system for efficient encapsulation and sustained release. OA pain arises largely from peripheral sensitization driven by inflammatory mediators within the joint. NSTX provides potent and reversible inhibition of voltage-gated sodium channels, particularly Nav1.7—a critical mediator of nociceptive signaling—without inducing long-term toxicity or neuroplastic changes, even at elevated doses.[12,13,15,19,20,47,48] As a site-1 sodium channel blocker, NSTX binds with high affinity at the outer pore to occlude ion permeation, a blockade that is fully reversible. Compared to related toxins such as saxitoxin (STX) and tetrodotoxin (TTX), NSTX demonstrates superior potency and a more favorable safety profile, including reduced neuronal and cardiac toxicity.[18,20] Preclinical and early clinical studies consistently show no evidence of chronic neurotoxicity or persistent channel dysfunction.[21,22] These features position NSTX as a particularly compelling candidate for OA pain management, where safe, localized, and reversible long-term analgesia is urgently needed. While other sustained delivery strategies for site-1 sodium channel blockers—including liposomes, supramolecular assemblies, and aptamer-based trapping—have yielded only modest extensions of block duration, typically limited to hours, our AlgPLGA-MP platform aims to overcome this barrier and enable durable pain relief.[48–52]

Our *in vivo* studies showed that IA injection of free NSTX at low doses produced only transient pain relief in both DMM mice and ACLT rats, and even a 100-fold dose increase failed to extend the duration of effect (Fig. 1C and D). These results highlight the need for a sustained-release system to maintain therapeutic levels within the joint and extend the analgesic benefit. Because IA delivery of NSTX has not been previously evaluated for OA pain, we tested its efficacy in DMM mice and ACLT rats. Demonstrating consistent effects across both models reduces the risk of species-specific artifacts, strengthens the evidence for generalizability, and better reflects the multifaceted nature of clinical OA pain, which involves both sensory and functional impairments. To address the formulation challenges of delivering a hydrophilic, cationic small molecule such as NSTX, we developed AlgPLGA-MP microparticles using a water-in-oil-in-water (W/O/W) double emulsion method.

The use of alginate in the internal aqueous phase improved encapsulation efficiency by promoting electrostatic interactions between negatively charged alginate and the positively

charged guanidinium groups of NSTX.[37,53] Calcium-mediated crosslinking further stabilized the alginate to form a solidified core, reducing initial burst release and improving drug retention. Encapsulation efficiency peaked at 2% (w/v) alginate, whereas beyond this concentration, high viscosity impaired emulsification efficiency (Fig. 3A). This highlights the importance of balancing electrostatic interactions and formulation rheology to optimize loading of charged hydrophilic molecules.

The resulting NSTX-AlgPLGA-MP formulation exhibited sustained *in vitro* release for over a month and preserved the chemical stability and sodium channel–blocking activity of NSTX. We developed the IMPRESSIVE assay—a fluorescence-based platform for assessing sodium channel inhibition—using Neuro-2a neuroblastoma cells, a sodium channel rich cell line well established in the literature as a sensitive and reproducible system for detecting sodium channel blockade. The assay demonstrated dose-dependent, reversible inhibition, confirming that NSTX retained its bioactivity after encapsulation and remained non-cytotoxic (Fig. 4D and Video S1, SI). *In vivo*, a single IA injection of NSTX-AlgPLGA-MP in a chronic OA mouse model resulted in significant pain relief for approximately one week, with elevated withdrawal thresholds observed through day 11 (Fig. 5A). An early peak in analgesia at 1.5 hours post-injection mirrored that of the free drug, indicating a small initial burst. The decline in efficacy beyond one week, despite a sustained *in vitro* release profile, suggests that clearance of microparticles from the joint likely contributes to reduced local drug concentration over time.

Many joint tissues, particularly cartilage, possess a high fixed negative charge density.[24] As a result, negatively charged particles are repelled by the matrix, remain suspended in synovial fluid, and undergo rapid clearance—a process further accelerated in inflamed joints where increased drainage and lymphatic flow limit drug bioavailability.[23,25,54,55] To overcome this barrier, we engineered AlgPLGA-MP with a cationic surface coating by conjugating avidin (AvAlgPLGA-MP). Avidin, a positively charged protein, enhances binding to glycosaminoglycans and other anionic ECM components, thereby promoting matrix attachment and prolonging intra-articular retention.[44,46,56] Electrostatic interactions of this kind are a well-established strategy for reducing particle clearance and extending joint residence time.[57–59] In our formulation, avidin was conjugated post-fabrication using DSPE-PEG-biotin incorporated during the second emulsion step.[46,59–61]

This surface modification reversed the net zeta potential of the particles from −26.4 ± 5.8 mV to +20.1 ± 10.4 mV at a 50% molar avidin-to-biotin ratio (Fig. 6C and Table 2). The positive surface charge facilitated electrostatic binding to negatively charged extracellular matrix components in the synovial fluid, such as hyaluronic acid (HA) and glycosaminoglycans (GAGs).[23,57,62–65] As a result, AvAlgPLGA-MP exhibited significantly enhanced joint residence time—retaining the intra-articular fluorescence signal for up to two weeks, as confirmed by IVIS imaging (Fig. 6D). The delayed increase in fluorescence intensity likely reflects a gradual release of encapsulated Cy7 dye, aided by aggregation-caused quenching (ACQ), which allowed for visualization of retained particles rather than free dye.[66,67] Despite improved retention, avidin modification reduced NSTX encapsulation, with up to 80% drug loss observed during DSPE-PEG-biotin incorporation and avidin conjugation steps (Fig. S4, SI). The reduced encapsulation efficiency (EE%) observed with AvAlgPLGA-MP is primarily attributable to the PEG moieties in DSPE-PEG-biotin. Because NSTX is a small, highly hydrophilic molecule, it readily partitions into hydrophilic PEG domains during formulation, resulting in drug loss. Similar effects have been reported in other systems: blending PEG-PLGA with PLGA lowered small-molecule encapsulation, and PEGylated PLGA microspheres loaded with 5-fluorouracil exhibited faster release and reduced EE%.[68,69] Compounding this issue, the organic solvent used in our formulation (DCM) has minimal solubility for NSTX; thus, once NSTX diffuses into PEG domains, inefficient recapture in the organic phase exacerbates drug loss.[38] Even after increasing the initial NSTX input, the encapsulated drug content remained slightly lower (Table 2). PEG-containing microspheres also tend to be more porous and absorb more water, further accelerating the release profile and lowering EE%.[70] Together with *in vivo* clearance, these factors raise concerns about whether sufficient intra-articular doses could be reliably achieved for meaningful analgesic studies. To offset this limitation, additional strategies—such as employing less hydrophilic linkers (*e.g.*, palmitic acid–avidin conjugates)—should be employed in the future to further improve loading efficiency and reduce manufacturing losses (Table 2).[71]

Importantly, we found no safety concerns with the use of cationic avidin for joint delivery. The dose of avidin used in our AvAlgPLGA-MP formulation in rats is 5 μM, which is significantly lower than the concentrations tested in our previous studies (up to 100 μM), where we observed no adverse effects on cartilage.[43,45,72] Specifically, we saw no change in GAG loss, chondrocyte viability, or biosynthesis rates of proteins and GAGs. Additionally, no immunogenic response was noted with 100 μM or lower dose in rats or rabbits.[43,45,56,73] Histopathological analyses of cartilage and synovium following AvAlgPLGA-MP injection further confirmed joint tissue biocompatibility in this study. Avidin has also been evaluated in human clinical trials. In a prospective Phase III substudy, a 30 minute intravenous infusion of 100 mg avidin was found to be well tolerated and safe in patients receiving biotinylated drugs for deep vein thrombosis.[74] Prior Phase I studies involving single or repeated intravenous doses of 25–100 mg avidin reported only a low incidence of asymptomatic antibody responses, with no cases of hypersensitivity.[75] These clinical findings further support the safety and translational potential of avidin as a surface modifier for intra-articular drug delivery.

Sustained-release intra-articular formulations are emerging as an important strategy in OA management, since most current therapies provide only short-term relief and require repeated injections. By maintaining therapeutic levels locally for about a week, our NSTX-loaded formulation offers meaningful extension of analgesic benefit compared with free drug

delivery. Such approaches can improve patient compliance, reduce injection burden, and minimize systemic exposure. The recent clinical success of Zilretta—an extended-release triamcinolone acetonide product formulated in PLGA microspheres—demonstrates the translational potential of sustained intra-articular delivery systems and has paved the way for similar PLGA-based platforms to enter the market.[76,77] These advances underscore the opportunity to leverage sustained-release technologies for safer, localized, and more effective long-term pain management in OA.

At the same time, it is critical to recognize that while sustained-release analgesics like NSTX may provide prolonged pain relief, they do not directly modify the underlying disease. This raises the possibility that effective symptom control, if uncoupled from structural protection, could encourage joint overuse and accelerate OA progression. A similar concern has been documented in clinical trials of anti-NGF antibody therapies, where profound analgesia without disease modification was linked to cases of rapidly progressive OA (RPOA), particularly at higher doses or when combined with NSAIDs.[78] These observations highlight the importance of pairing effective pain relief with strategies that preserve joint integrity. Looking ahead, the most promising therapeutic paradigm will likely emphasize combinatorial approaches that integrate analgesia with disease-modifying interventions. Within this framework, transient and reversible sodium channel blockade is especially attractive, as it provides robust pain relief without inducing permanent neuronal alterations that could complicate long-term treatment.

In conclusion, this study demonstrates that NSTX is a potent analgesic for OA-associated pain but is limited by rapid joint clearance and short therapeutic duration when delivered as a free drug. Encapsulation in AlgPLGA-MP substantially extended pain relief to one week, while avidin surface modification further prolonged joint residence time and holds promise for extending analgesic duration even further. Future work will focus on optimizing the AvAlgPLGA-MP formulation to minimize aggregation and improve drug loading efficiency to enable effective, single dose administration essential for clinical use. Given its modular nature, this platform is also adaptable for co-delivery of OA biologics and small-molecule analgesics, offering a promising strategy for combination therapies that address both symptom relief and joint regeneration.

Author contributions

HZ designed and implemented all the experiments and wrote the manuscript. HMB and CZ supported formulation optimization and biological experiments. *In vivo* mouse experiments were designed by REM and performed by JL, SI, and NSA. EMC provided guidance and expertise in experimental design. AGB conceived the idea, procured funding, designed experiments, and oversaw data analysis and writing of the manuscript. All authors were involved in writing, reviewing, and approving the final version of the manuscript.

Conflicts of interest

There are no conflicts to declare.

Data availability

The data that support the findings of this study are openly available in Figshare at https://doi.org/10.6084/m9.figshare.29522009, reference number 29522009.

Supplementary information (SI) is available. See DOI: https://doi.org/10.1039/d5nr02912k.

Acknowledgements

This work was supported by the National Institutes of Health (NIH) R01AR075121, R01AR075121-S1 and R01AR077019, and Tufts Clinical and Translational Science Institute (CTSI) Award 5UL1TR002544. The authors would like to acknowledge Dr Anne-Marie Malfait and the Chicago Center on Musculoskeletal Pain Research Core Center for support of the mouse experiments (funded by NIH NIAMS P30AR079206; resources can be requested at https://mskpain.center/). The authors would like to thank Boston Electron Microscopy Core, Northeastern University, for offering TEM, and Institute for Chemical Imaging of Living Systems (CILS), Northeastern University, for offering confocal microscopy. The authors would also like to thank Dr Nitin Joshi from Brigham and Women's Hospital, Harvard Medical School, for gifting the Neuro-2a cell line.

References

1 J. Dahlhamer, *et al.*, Prevalence of Chronic Pain and High-Impact Chronic Pain Among Adults—United States, 2016, *Morb. Mortal. Wkly. Rep.*, 2018, **67**, 1001–1006.
2 D. A. Queremel Milani and D. D. Davis, Pain Management Medications, in *StatPearls*, StatPearls Publishing, Treasure Island (FL), 2025.
3 A.-M. Malfait, R. E. Miller and R. J. Miller, Basic Mechanisms of Pain in Osteoarthritis, *Rheum. Dis. Clin. North Am.*, 2021, **47**, 165–180.
4 N. Schuelert and J. J. McDougall, Involvement of Nav 1.8 sodium ion channels in the transduction of mechanical pain in a rodent model of osteoarthritis, *Arthritis Res. Ther.*, 2012, **14**, R5.
5 S. Lolignier, *et al.*, Nav1.9 Channel Contributes to Mechanical and Heat Pain Hypersensitivity Induced by Subacute and Chronic Inflammation, *PLoS One*, 2011, **6**, e23083.

6 W. Fu, *et al.*, Nav1.7 as a chondrocyte regulator and therapeutic target for osteoarthritis, *Nature*, 2024, **625**, 557–565.
7 P. Beninger, Journavx (suzetrigine), *Clin. Ther.*, 2025, **47**, 400–401.
8 G. M. Lipkind and H. A. Fozzard, A structural model of the tetrodotoxin and saxitoxin binding site of the Na+ channel, *Biophys. J.*, 1994, **66**, 1–13.
9 M. Stevens, S. Peigneur and J. Tytgat, Neurotoxins and Their Binding Areas on Voltage-Gated Sodium Channels, *Front. Pharmacol.*, 2011, **2**, 71.
10 H. Pajouhesh, *et al.*, Discovery of a selective, state-independent inhibitor of NaV1.7 by modification of guanidinium toxins, *Sci. Rep.*, 2020, **10**, 14791.
11 R. Mackieh, *et al.*, Voltage-Gated Sodium Channels: A Prominent Target of Marine Toxins, *Mar. Drugs*, 2021, **19**, 562.
12 W. A. Catterall and T. M. Swanson, Structural Basis for Pharmacology of Voltage-Gated Sodium and Calcium Channels, *Mol. Pharmacol.*, 2015, **88**, 141–150.
13 H. A. Fozzard, M. F. Sheets and D. A. Hanck, The Sodium Channel as a Target for Local Anesthetic Drugs, *Front. Pharmacol.*, 2011, **2**, 68.
14 P. N. Kao, M. R. James-Kracke and C. Y. Kao, The active guanidinium group of saxitoxin and neosaxitoxin identified by the effects of pH on their activities on squid axon, *Pflügers Arch. Eur. J. Physiol.*, 1983, **398**, 199–203.
15 G. Strichartz, Structural determinants of the affinity of saxitoxin for neuronal sodium channels. Electrophysiological studies on frog peripheral nerve, *J. Gen. Physiol.*, 1984, **84**, 281–305.
16 M. J. Su and M. Morad, Effects of quinidine and lidocaine on action potential and membrane currents of frog ventricles, *Proc. Natl. Sci. Counc., Repub. China, Part B*, 1987, **11**, 362–369.
17 F. Flenner, *et al.*, In Vitro Negative Inotropic Effect of Low Concentrations of Bupivacaine Relates to Diminished Ca2+ Sensitivity but Not to Ca2+ Handling or β-Adrenoceptor Signaling, *Anesthesiology*, 2018, **128**, 1175.
18 M. C. Wylie, *et al.*, Respiratory, Neuromuscular, and Cardiovascular Effects of Neosaxitoxin in Isoflurane-Anesthetized Sheep, *Reg. Anesth. Pain Med.*, 2012, **37**, 152–158.
19 J. Galindo, *et al.*, Long-lasting, reversible and non-neurotoxic inactivation of hippocampus activity induced by neosaxitoxin, *J. Neurosci. Methods*, 2018, **308**, 197–204.
20 R. J. Zepeda, M. Candiracci, N. Lobos, S. Lux and H. F. Miranda, Chronic Toxicity Study of Neosaxitoxin in Rats, *Mar. Drugs*, 2014, **12**, 5055–5071.
21 A. J. Rodriguez-Navarro, *et al.*, Neosaxitoxin as a Local Anesthetic: Preliminary Observations from a First Human Trial, *Anesthesiology*, 2007, **106**, 339–345.
22 K. Lobo, *et al.*, A Phase 1, Dose-escalation, Double-blind, Block-randomized, Controlled Trial of Safety and Efficacy of Neosaxitoxin Alone and in Combination with 0.2% Bupivacaine, with and without Epinephrine, for Cutaneous Anesthesia, *Anesthesiology*, 2015, **123**, 873.
23 A. G. Bajpayee and A. J. Grodzinsky, Cartilage-targeting drug delivery: Can electrostatic interactions help?, *Nat. Rev. Rheumatol.*, 2017, **13**, 183–193.
24 A. Vedadghavami, C. Zhang and A. G. Bajpayee, Overcoming negatively charged tissue barriers: Drug delivery using cationic peptides and proteins, *Nano Today*, 2020, **34**, 100898.
25 A. Selvadoss, H. M. Baby, H. Zhang and A. G. Bajpayee, Harnessing exosomes for advanced osteoarthritis therapy, *Nanoscale*, 2024, **16**, 19174–19191.
26 Y. Wang, B. Qin, G. Xia and S. H. Choi, FDA's Poly (Lactic-Co-Glycolic Acid) Research Program and Regulatory Outcomes, *AAPS J.*, 2021, **23**, 92.
27 J. Paik, S. T. Duggan and S. J. Keam, Triamcinolone Acetonide Extended-Release: A Review in Osteoarthritis Pain of the Knee, *Drugs*, 2019, **79**, 455–462.
28 F. Ramazani, *et al.*, Strategies for encapsulation of small hydrophilic and amphiphilic drugs in PLGA microspheres: State-of-the-art and challenges, *Int. J. Pharm.*, 2016, **499**, 358–367.
29 M. Ali, X. F. Walboomers, J. A. Jansen and F. Yang, Influence of formulation parameters on encapsulation of doxycycline in PLGA microspheres prepared by double emulsion technique for the treatment of periodontitis, *J. Drug Delivery Sci. Technol.*, 2019, **52**, 263–271.
30 A. Gaignaux, *et al.*, Development and evaluation of sustained-release clonidine-loaded PLGA microparticles, *Int. J. Pharm.*, 2012, **437**, 20–28.
31 Q. Xu, A. Crossley and J. Czernuszka, Preparation and characterization of negatively charged poly(lactic-co-glycolic acid) microspheres, *J. Pharm. Sci.*, 2009, **98**, 2377–2389.
32 Y. Kim, E. J. Park, T. W. Kim and D. H. Na, Recent Progress in Drug Release Testing Methods of Biopolymeric Particulate System, *Pharmaceutics*, 2021, **13**, 1313.
33 A. M. Obeidat, *et al.*, Intra-articular sprouting of nociceptors accompanies progressive osteoarthritis: comparative evidence in four murine models, *Front. Neuroanat.*, 2024, **18**, 1429124.
34 Y. Wang, *et al.*, Assessment of osteoarthritis functional outcomes and intra–articular injection volume in the rat anterior cruciate ligament transection model, *J. Orthop. Res.*, 2022, **40**, 2004–2014.
35 A. M. Obeidat, *et al.*, A standardized approach to evaluation and reporting of synovial histopathology in two surgically induced murine models of osteoarthritis, *Osteoarthr. Cartil.*, 2024, **32**, 1273–1282.
36 F. Y. Han, K. J. Thurecht, A. K. Whittaker and M. T. Smith, Bioerodable PLGA-Based Microparticles for Producing Sustained-Release Drug Formulations and Strategies for Improving Drug Loading, *Front. Pharmacol.*, 2016, **7**, 185.
37 M. P. A. Lim, W. L. Lee, E. Widjaja and S. C. J. Loo, One-step fabrication of core–shell structured alginate–PLGA/PLLA microparticles as a novel drug delivery system for water soluble drugs, *Biomater. Sci.*, 2013, **1**, 486.
38 A. Alfonso, M. C. Louzao, M. R. Vieytes and L. M. Botana, Comparative study of the stability of saxitoxin and neosaxi-

toxin in acidic solutions and lyophilized samples, *Toxicon*, 1994, **32**, 1593–1598.
39 E. Cagide, *et al.*, Hapalindoles from the Cyanobacterium *Fischerella* : Potential Sodium Channel Modulators, *Chem. Res. Toxicol.*, 2014, **27**, 1696–1706.
40 M. C. Louzao, *et al.*, The Sodium Channel of Human Excitable Cells is a Target for Gambierol, *Cell. Physiol. Biochem.*, 2006, **17**, 257–268.
41 R. L. Rungta, *et al.*, The Cellular Mechanisms of Neuronal Swelling Underlying Cytotoxic Edema, *Cell*, 2015, **161**, 610–621.
42 C. Zhang, T. He, A. Vedadghavami and A. G. Bajpayee, Avidin-biotin technology to synthesize multi-arm nano-construct for drug delivery, *MethodsX*, 2020, **7**, 100882.
43 T. He, I. Shaw, A. Vedadghavami and A. G. Bajpayee, Single-Dose Intra-Cartilage Delivery of Kartogenin Using a Cationic Multi-Arm Avidin Nanocarrier Suppresses Cytokine-Induced Osteoarthritis-Related Catabolism, *Cartilage*, 2022, **13**, 19476035221093072.
44 E. K. Wagner, *et al.*, Avidin grafted dextran nanostructure enables a month-long intra-discal retention, *Sci. Rep.*, 2020, **101**(10), 1–14.
45 T. He, *et al.*, Intra-articular kinetics of a cartilage targeting cationic PEGylated protein for applications in drug delivery, *Osteoarthr. Cartil.*, 2023, **31**, 187–198.
46 T. V. Pathrikar, *et al.*, Cartilage-targeting Exosomes for Delivery of Receptor Antagonist of Interleukin-1 in Osteoarthritis treatment, *Osteoarthr. Cartil.*, 2025, **33**, 835–847.
47 H. Yang, H. G. E. Meijer, R. J. Doll, J. R. Buitenweg and S. A. van Gils, Dependence of Nociceptive Detection Thresholds on Physiological Parameters and Capsaicin-Induced Neuroplasticity: A Computational Study, *Front. Comput. Neurosci.*, 2016, **10**, 49.
48 T. Ji, *et al.*, Delivery of local anaesthetics by a self-assembled supramolecular system mimicking their interactions with a sodium channel, *Nat. Biomed. Eng.*, 2021, **5**, 1099–1109.
49 H. Epstein-Barash, *et al.*, Prolonged duration local anesthesia with minimal toxicity, *Proc. Natl. Acad. Sci. U. S. A.*, 2009, **106**, 7125–7130.
50 D. Wang, *et al.*, An aptamer-based depot system for sustained release of small molecule therapeutics, *Nat. Commun.*, 2023, **14**, 2444.
51 C. Zhao, *et al.*, Polymer-tetrodotoxin conjugates to induce prolonged duration local anesthesia with minimal toxicity, *Nat. Commun.*, 2019, **10**, 2566.
52 D. S. Kohane, *et al.*, Prolonged duration local anesthesia from tetrodotoxin-enhanced local anesthetic microspheres, *Pain*, 2003, **104**, 415–421.
53 J. Wu, *et al.*, Fabrication and characterization of monodisperse PLGA–alginate core–shell microspheres with monodisperse size and homogeneous shells for controlled drug release, *Acta Biomater.*, 2013, **9**, 7410–7419.
54 P. Maudens, O. Jordan and E. Allémann, Recent advances in intra-articular drug delivery systems for osteoarthritis therapy, *Drug Discovery Today*, 2018, **23**, 1761–1775.
55 S. Mehta, T. He and A. G. Bajpayee, Recent advances in targeted drug delivery for treatment of osteoarthritis, *Curr. Opin. Rheumatol.*, 2021, **33**, 94–109.
56 T. L. Boyer, *et al.*, Cartilage targeting cationic peptide carriers display deep cartilage penetration and retention in a rabbit model of post-traumatic osteoarthritis, *Osteoarthr. Cartil.*, 2025, **33**, 721–734.
57 M. Morgen, *et al.*, Nanoparticles for Improved Local Retention after Intra-Articular Injection into the Knee Joint, *Pharm. Res.*, 2013, **30**, 257–268.
58 B. Hakim, T. L. Boyer, S. Chakraborty and A. G. Bajpayee, Spatial Charge-Hydrophobicity Configuration Modulates Cationic Peptide Transport in Cartilage, *Biophys. J.*, 2025, DOI: 10.1016/j.bpj.2025.09.023.
59 C. Zhang, *et al.*, Charge-Reversed Exosomes for Targeted Gene Delivery to Cartilage for Osteoarthritis Treatment, *Small Methods*, 2024, **8**, 2301443.
60 H. A. Millán Cotto, *et al.*, Cationic-motif-modified exosomes for mRNA delivery to retinal photoreceptors, *J. Mater. Chem. B*, 2024, **12**, 7384–7400.
61 C. Zhang, *et al.*, Milk exosomes anchored with hydrophilic and zwitterionic motifs enhance mucus permeability for applications in oral gene delivery, *Biomater. Sci.*, 2024, **12**, 634–649.
62 A. G. Bajpayee, M. Scheu, A. J. Grodzinsky and R. M. Porter, Electrostatic interactions enable rapid penetration, enhanced uptake and retention of intra-articular injected avidin in rat knee joints, *J. Orthop. Res. Off. Publ. Orthop. Res. Soc.*, 2014, **32**, 1044–1051.
63 A. G. Bajpayee, M. A. Quadir, P. T. Hammond and A. J. Grodzinsky, Charge based intra-cartilage delivery of single dose dexamethasone using Avidin nano-carriers suppresses cytokine-induced catabolism long term, *Osteoarthr. Cartil. OARS Osteoarthr. Res. Soc.*, 2016, **24**, 71–81.
64 A. G. Bajpayee, M. Scheu, A. J. Grodzinsky and R. M. Porter, A rabbit model demonstrates the influence of cartilage thickness on intra-articular drug delivery and retention within cartilage, *J. Orthop. Res.*, 2015, **33**, 660–667.
65 A. G. Bajpayee, C. R. Wong, M. G. Bawendi, E. H. Frank and A. J. Grodzinsky, Avidin as a model for charge driven transport into cartilage and drug delivery for treating early stage post-traumatic osteoarthritis, *Biomaterials*, 2014, **35**, 538–549.
66 R. Sangsuwan, *et al.*, Intra-articular injection of flavopiridol-loaded microparticles for treatment of post-traumatic osteoarthritis, *Acta Biomater.*, 2022, **149**, 347–358.
67 L. Jiao, *et al.*, Constructing a Local Hydrophobic Cage in Dye-Doped Fluorescent Silica Nanoparticles to Enhance the Photophysical Properties, *ACS Cent. Sci.*, 2020, **6**, 747–759.
68 M. M. El-Hammadi, Á.V Delgado, C. Melguizo, J. C. Prados and J. L. Arias, Folic acid-decorated and PEGylated PLGA nanoparticles for improving the antitumour activity of 5-fluorouracil, *Int. J. Pharm.*, 2017, **516**, 61–70.
69 M. Hussain, *et al.*, Regulation of Drug Release by Tuning Surface Textures of Biodegradable Polymer Microparticles, *ACS Appl. Mater. Interfaces*, 2017, **9**, 14391–14400.

70 J. Buske, *et al.*, Influence of PEG in PEG–PLGA microspheres on particle properties and protein release, *Eur. J. Pharm. Biopharm.*, 2012, **81**, 57–63.
71 T. M. Fahmy, R. M. Samstein, C. C. Harness and W. Mark Saltzman, Surface, modification of biodegradable polyesters with fatty acid conjugates for improved drug targeting, *Biomaterials*, 2005, **26**, 5727–5736.
72 T. He, *et al.*, Multi-arm Avidin nano-construct for intra-cartilage delivery of small molecule drugs, *J. Controlled Release*, 2020, **318**, 109–123.
73 A. Bajpayee, *et al.*, Sustained intra-cartilage delivery of low dose dexamethasone using a cationic carrier for treatment of post traumatic osteoarthritis, *Eur. Cell. Mater.*, 2017, **34**, 341–364.
74 I. Paty, *et al.*, Reversibility of the anti–FXa activity of idrabiotaparinux (biotinylated idraparinux) by intravenous avidin infusion, *J. Thromb. Haemostasis*, 2010, **8**, 722–729.
75 M. Trellu, *et al.*, Bioequipotency of idraparinux and idrabiotaparinux after once weekly dosing in healthy volunteers and patients treated for acute deep vein thrombosis, *Br. J. Clin. Pharmacol.*, 2013, **75**, 1255–1264.
76 N. A. Segal and J. C. Alm, The effect of intra-articular extended-release triamcinolone acetonide on OARSI-recommended physical performance measures in adults with bilateral symptomatic knee osteoarthritis, *Osteoarthr. Cartil. Open*, 2022, **4**, 100268.
77 P. G. Conaghan, *et al.*, Effects of a Single Intra-Articular Injection of a Microsphere Formulation of Triamcinolone Acetonide on Knee Osteoarthritis Pain, *J. Bone Jt. Surg., Am. Vol.*, 2018, **100**, 666–677.
78 B. W. Dietz, M. C. Nakamura, M. T. Bell and N. E. Lane, Targeting Nerve Growth Factor for Pain Management in Osteoarthritis—Clinical Efficacy and Safety, *Rheum. Dis. Clin. North Am.*, 2021, **47**, 181–195.